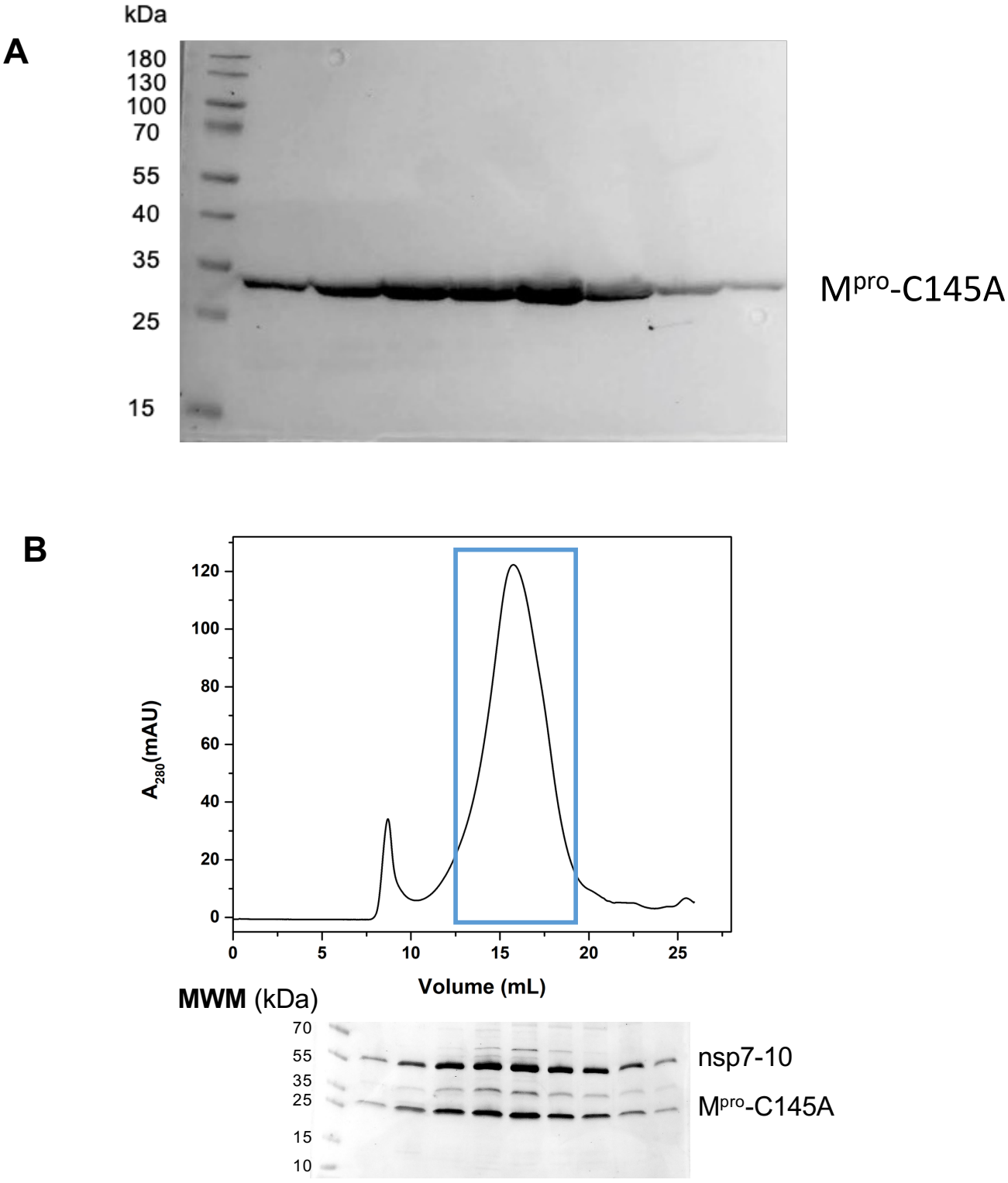

Figure S1 (A) Purification of M^{pro}-C145A by size exclusion chromatography. (B) Purification of the M^{pro}-C145A and nsp7-10 complex by size exclusion chromatography (top). SDS-PAGE analysis confirmed peak fractions (blue line boxed) containing both M^{pro} and nsp7-10 (bottom).

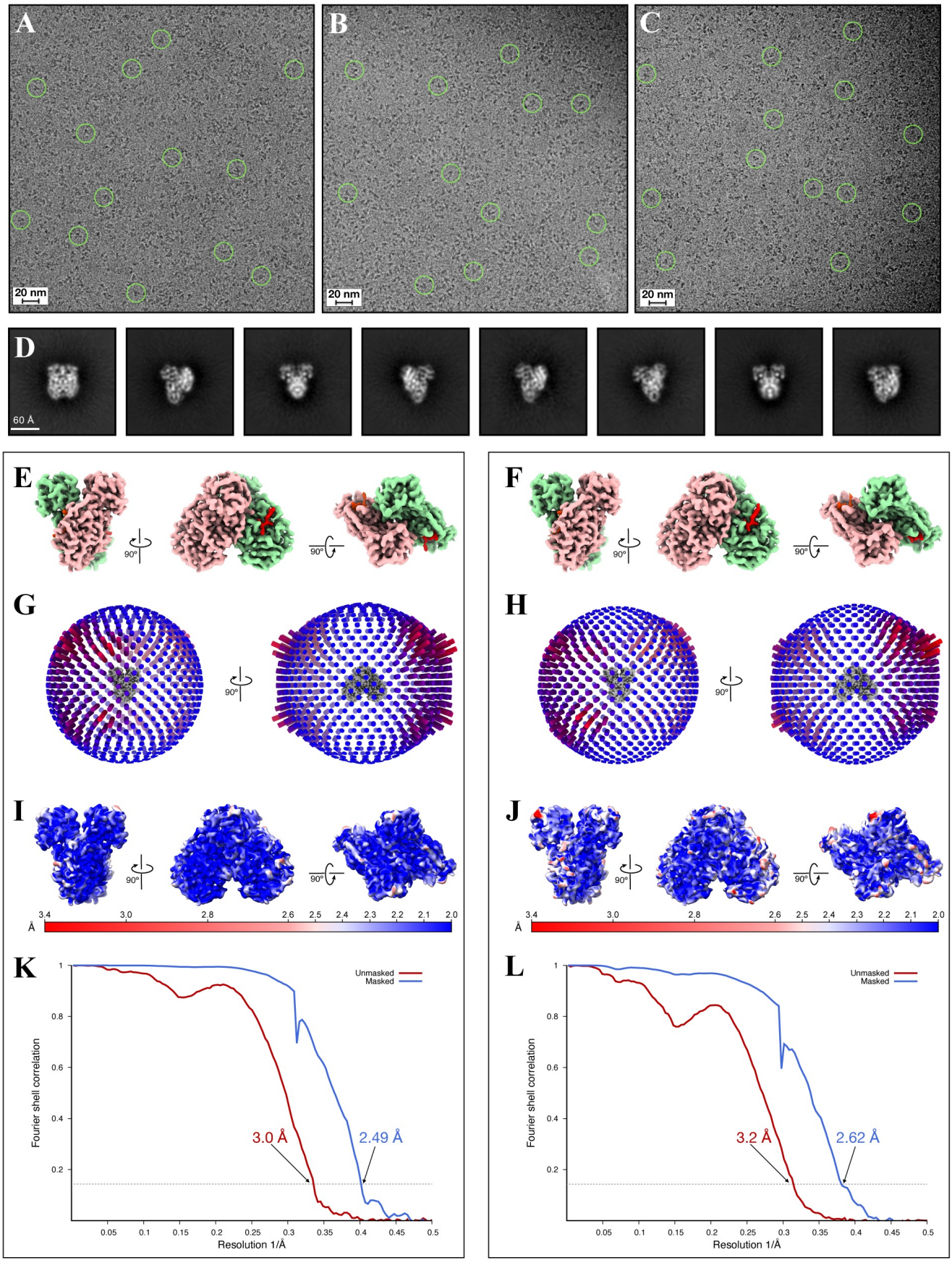

Figure S2. Cryo-EM data processing for the 3D reconstruction of the M^{pro}-C145A-nsp7-10 complex as C2 (panels E,G,I,K) and C1 symmetries (panels F,H,J,L), respectively. (A-C) Representative cryo-EM micrograph. (D) 2D-class averages. (E,F) density maps calculated for the complex. (G,H) Angular distribution of reconstructed particles in the refined maps. (I,J) Local resolution maps calculated by Phenix. Both maps use the same color key in Å. (K,L) FSC plots of unmasked and masked maps.

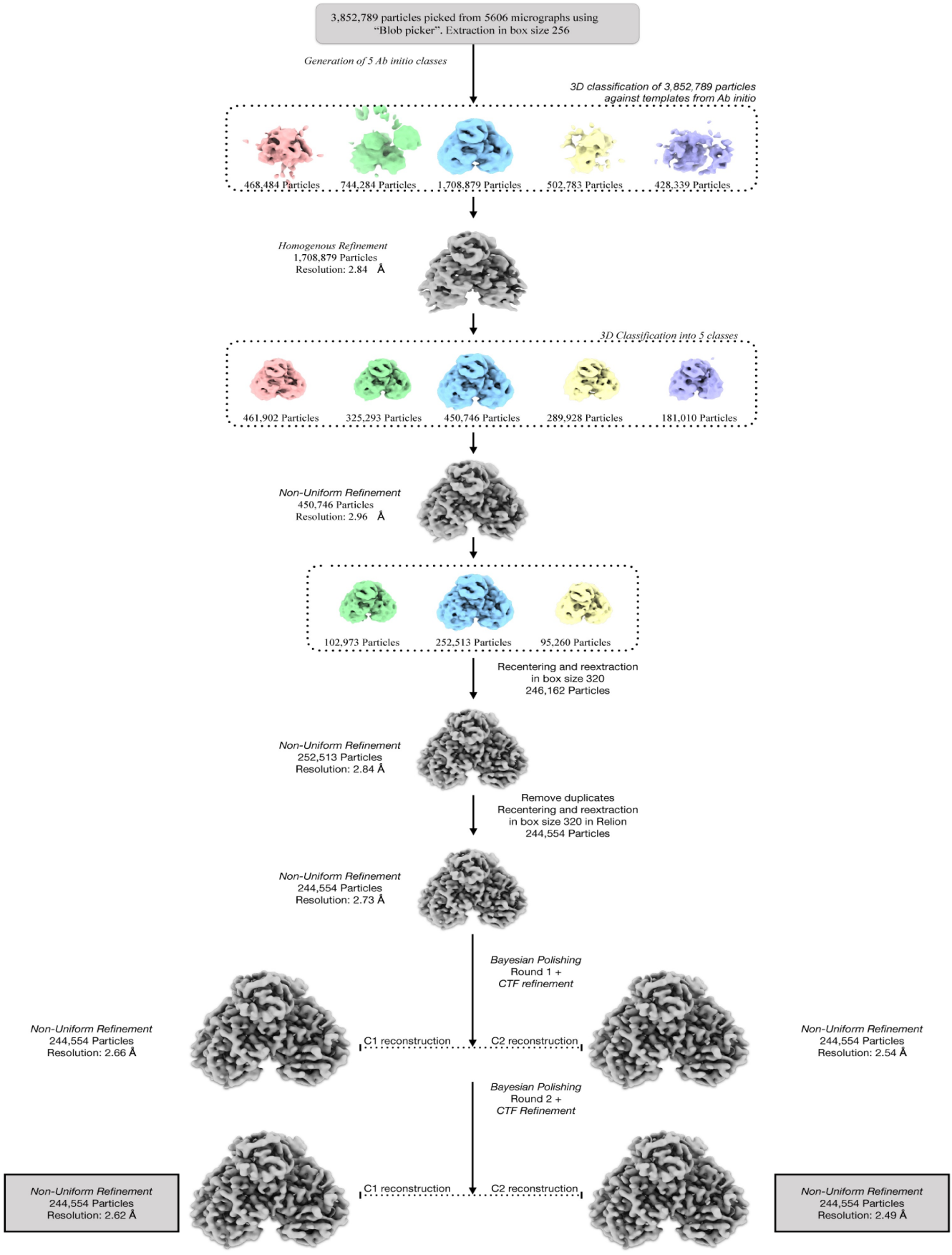

Figure S3. M^{pro}-C145A-nsp7-10 cryo-EM data processing summary. The flowchart shows the main steps in the data processing, from particle picking, through classification, to final maps. A selected subset of the initial reference-free 2D class averages and all the intermediate 3D class averages computed during the processing of this dataset are shown. Further attempts to process the discarded classes are omitted from this chart for clarity, as these data did not contribute to the final particle set.

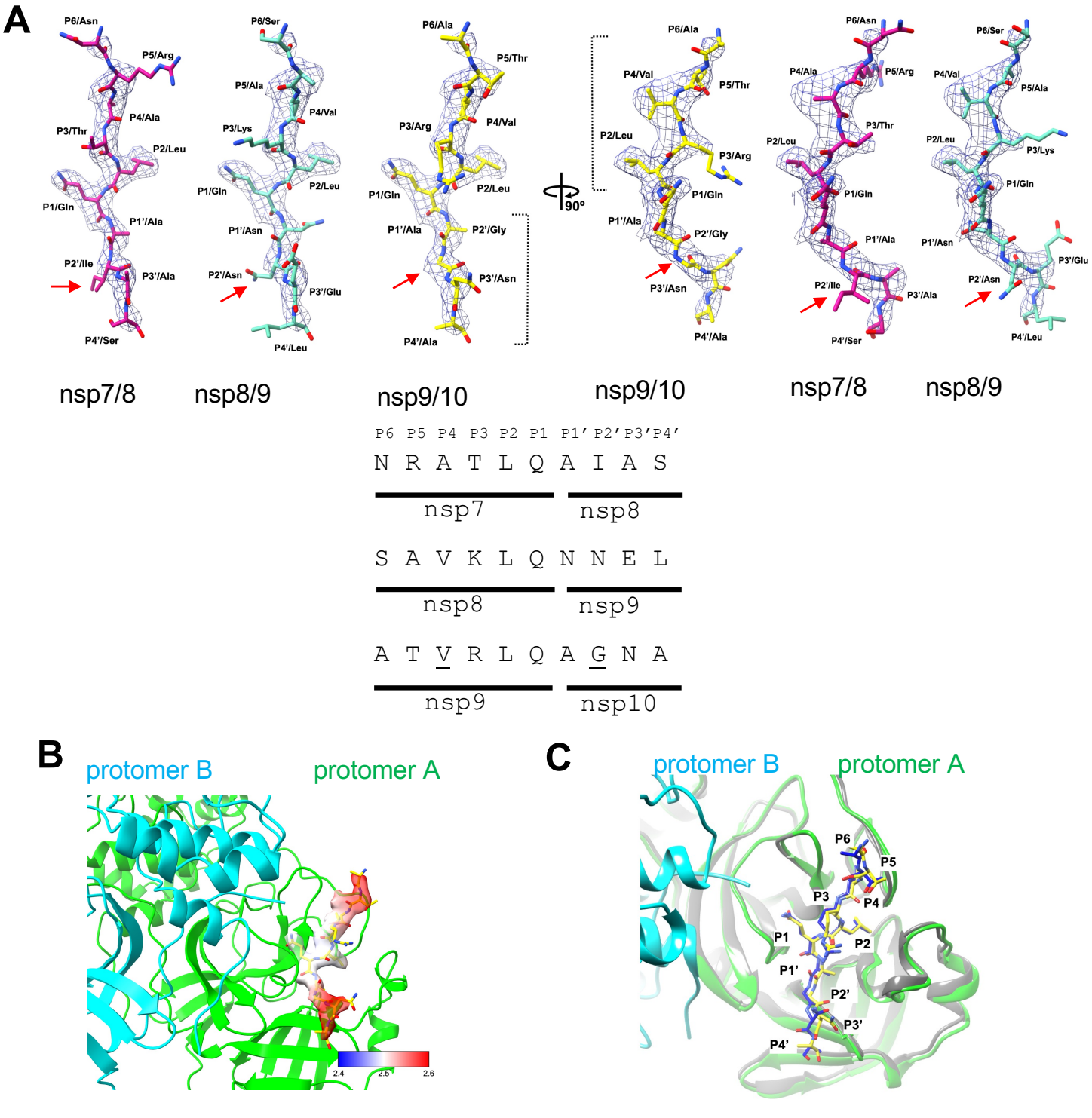

Figure S4. (A) Fitting the M^{pro} recognition sites found in nsp7-10 polyprotein including nsp7/8, nsp8/9 and nsp9/10 on the cryo-EM density map of the M^{pro}-C145A and nsp7-10 complex. Larger amino acid side chains at the P2' position of nsp7/8 (Ile) and nsp8/9 (Asn) sites do not fit to the cryo-EM density map (red arrows) compared with the nsp9/10 site (Gly). The amino acid sequences of the M^{pro} recognition site are listed below. (B) Local resolution estimation (2.4~2.6 Å) of the peptide density bound at the M^{pro}-C145A active site. A difference map representing the peptide bound at the active site was calculated by first computing a model map using M^{pro} without peptide and then subtracting it from the cryo-EM map of M^{pro} and nsp7-10 complex. (C) Comparing the binding of nsp9/10 recognition site at the M^{pro} active site investigated by the cryo-EM (this study, nsp9/10, yellow; M^{pro}, green) and X-ray crystallography (PDB: 7DVY, nsp9/10, blue; M^{pro}, gray).

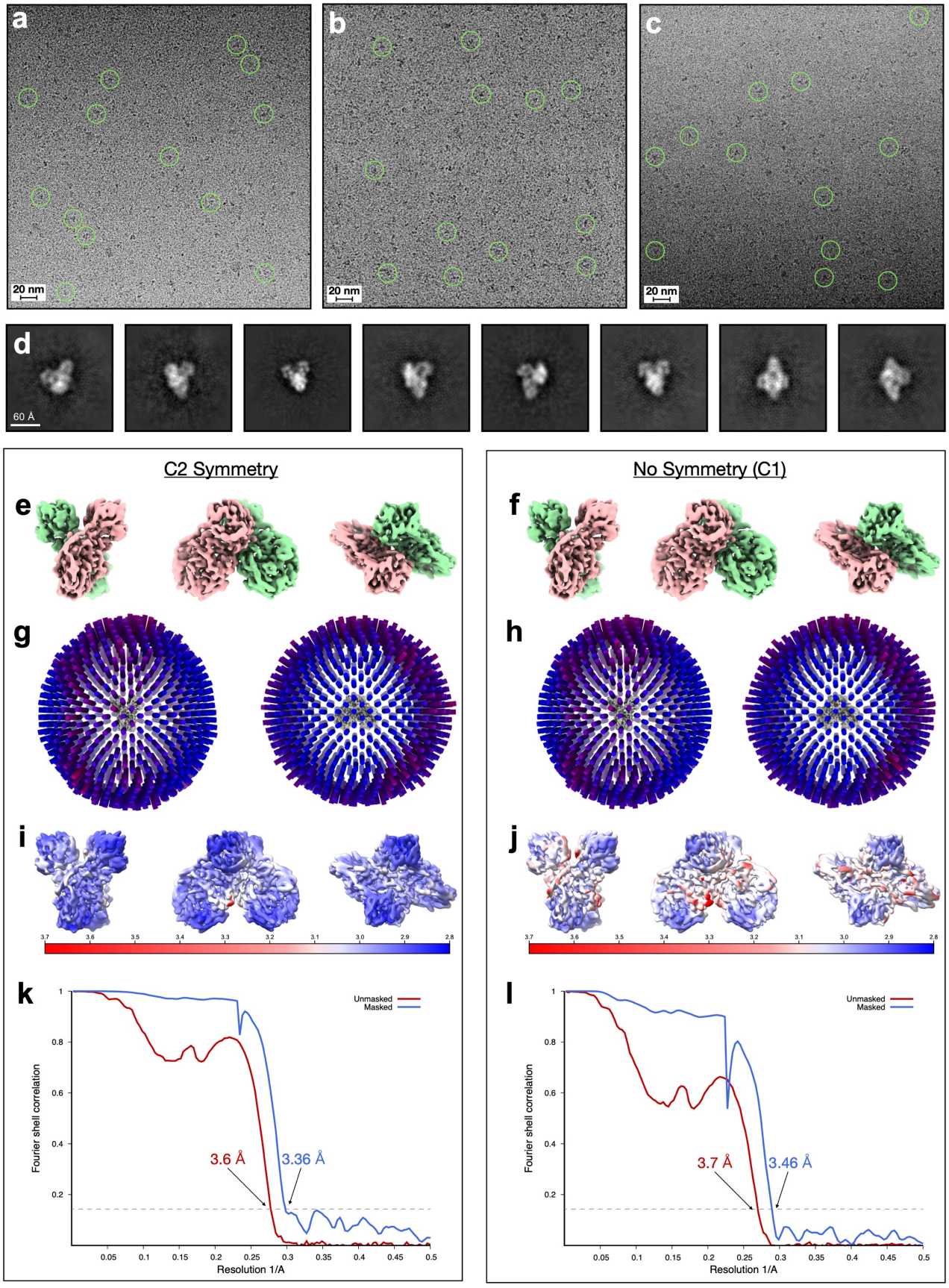

Figure S5. Cryo-EM data processing for the 3D reconstruction of wild-type M^{pro} as C2 (panels e,g,i,k) and C1 symmetories (panels f,h,j,l), respectively. (a-c) Representative cryo-EM micrograph. (d) 2D-class averages. (e,f) density maps calculated for the complex. (g,h) Angular distribution of reconstructed particles in the refined maps. (I,j) Local resolution maps calculated by Phenix. Both maps use the same color key, in Å. (k,l) FSC plots of unmasked and masked maps.

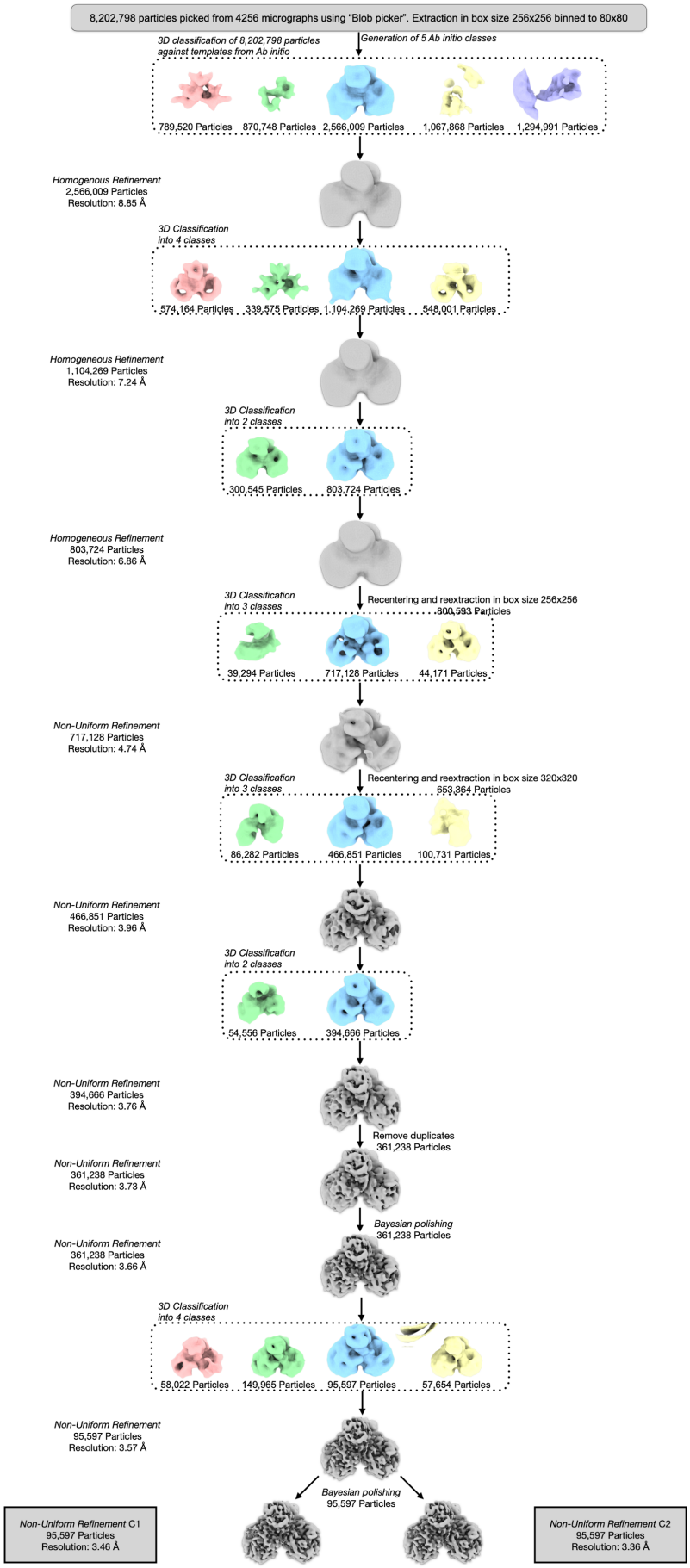

Figure S6. Wild-type M^{pro} cryo-EM data processing. The flowchart shows the main steps in the data processing, from particle picking, through classification, to final maps. A selected subset of the initial reference-free 2D class averages and all the intermediate 3D class averages computed during the processing of this dataset are shown.

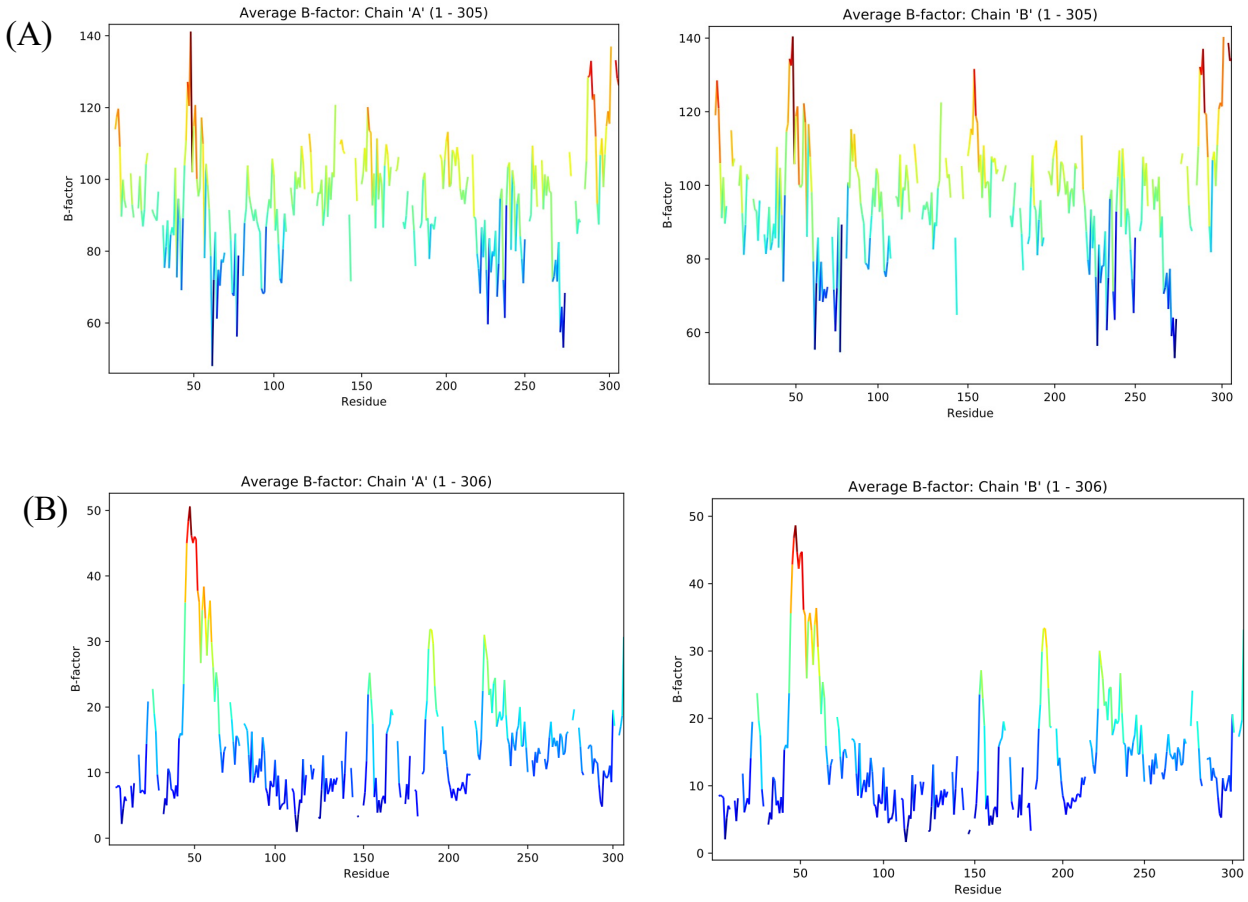

Figure S7. Comparison of B-factor average of cryo-EM derived M^{pro} protease in apo (A) and the complex with nsp7-10 polyprotein (B).

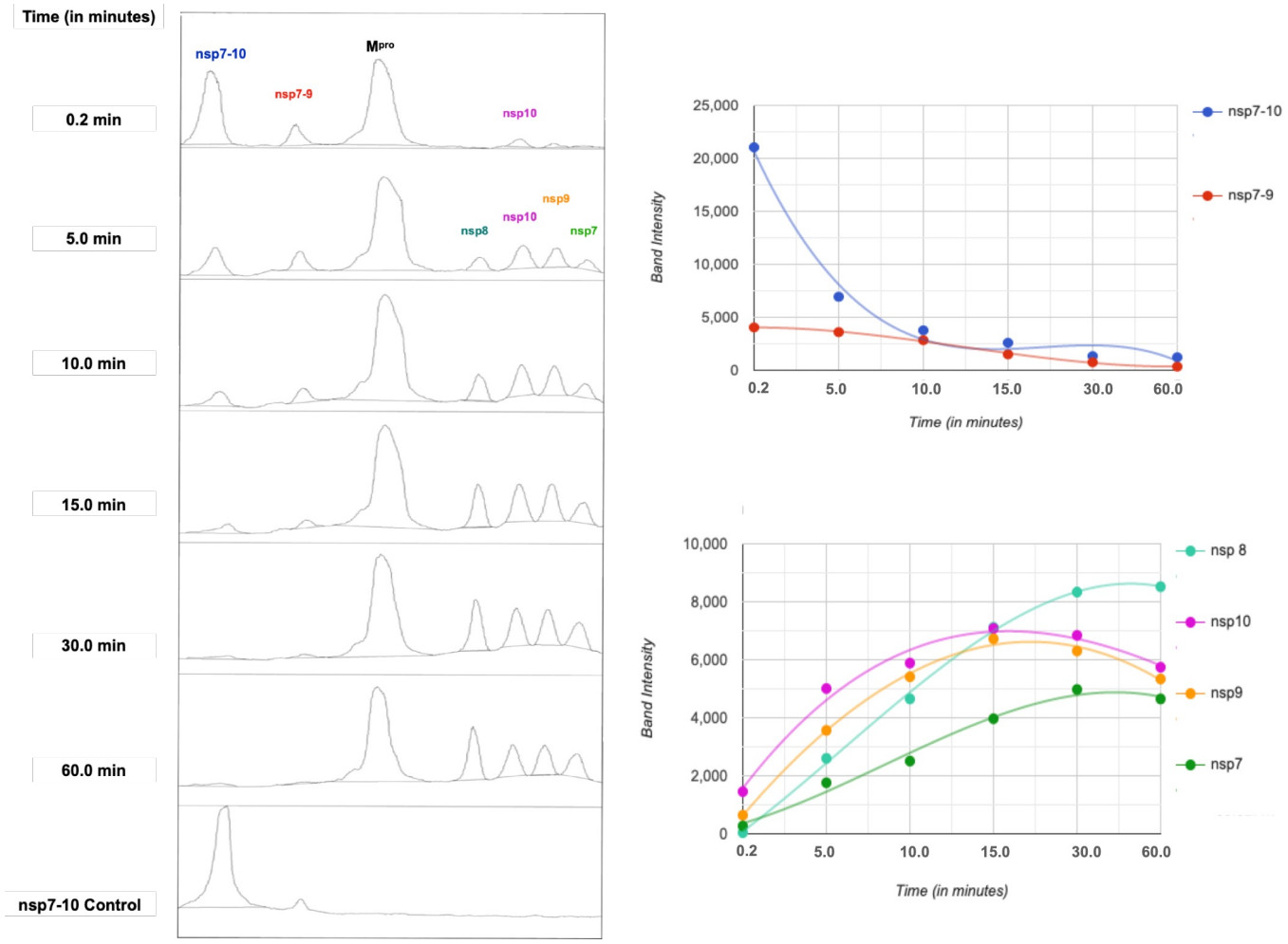

Figure S8. Quantification of limited protease assay from Figure 1B using ImageJ (A) Intensity change for the nsp7-10, intermediate and final products are measured as peaks and plotted (B) using ScatterPlot from Rapidtables (https://www.rapidtables.com/tools/scatter-plot.html).